Ultra-high resistive switching mechanism induced by oxygen ion accumulation on nitrogen-doped resistive random access memory

Tian-Jian Chu,[1] Tsung-Ming Tsai,[1,a)] Ting-Chang Chang,[2,a)] Kuan-Chang Chang,[1] Chih-Hung Pan,[1] Kai-Huang Chen,[3] Jung-Hui Chen,[4] Hsin-Lu Chen,[5] Hui-Chun Huang,[1] Chih-Cheng Shih,[1] Yong-En Syu,[2] Jin-Cheng Zheng,[6] and Simon M. Sze[2]

[1]*Department of Materials and Optoelectronic Science, National Sun Yat-Sen University, No. 70 Lien-Hai Rd., Kaohsiung 80424, Taiwan*
[2]*Department of Physics, National Sun Yat-Sen University, No. 70 Lien-Hai Rd., Kaohsiung 80424, Taiwan*
[3]*Department of Electronics Engineering and Computer Science, Tung-Fang Design Institute, Kaohsiung 82941, Taiwan*
[4]*Department of Chemistry, National Kaohsiung Normal University, Kaohsiung, 82446, Taiwan*
[5]*Department of Mechanical and Electro-Mechanical Engineering, National Sun Yat-Sen University, No. 70 Lien-Hai Rd., Kaohsiung 80424, Taiwan*
[6]*Department of Physics, Xiamen University, No. 422, Siming South Road, Xiamen, Fujian 361005, China*

(Received 15 September 2014; accepted 7 November 2014; published online 5 December 2014)

This study presents the dual bipolar resistive switching characteristics induced by oxygen-ion accumulation. By introducing nitrogen to the interface between the resistive switching region and active switching electrode, filament-type and interface-type resistive switching behaviors can both exist under different operation conditions. This particular oxygen-ion accumulation-induced switching behavior suggests an extraordinary potential for resistive random access memory applications because the operating power can be significantly decreased (about 100 times). The physical mechanism of this oxygen-ion accumulation-induced interface-type resistive switching behavior is explained by our model and clarified by current conduction mechanism and material analysis. © *2014 AIP Publishing LLC*. [http://dx.doi.org/10.1063/1.4902503]

In the development of the IT industry in the next generation, including forward-looking consumer electronics and an Internet of things (IoT), non-volatile memory (NVM) will play a decisive role in this wave of change.[1–5] Currently, non-volatile flash memory has been widely applied in electronic devices. However, flash memory faces challenges to its technical and physical limits. Therefore, next generation nonvolatile memories have been extensively researched, including phase change to random access memory (PCRAM), magnetic random access memory (MRAM), ferroelectric random access memory (FeRAM), and resistive random access memory (RRAM). Among these, RRAM is the most promising candidate due to its very low operation voltage, extremely fast write/erase speeds, and excellent scaling capability.[6–35]

Various materials have been reported to possess resistive switching behaviors. However, silicon oxide-based ones are promising for RRAM applications because of their great compatibility in integrated circuit (IC) processes. In our previous work, metal-doped silicon oxide ($M:SiO_x$) co-sputtered at room temperature for use as a resistive switching layer has been studied. We reported a bipolar switching behavior and outstanding performance, including over 10^6 cycles of endurance and excellent retention under high temperature.[36–42]

In this paper, sandwiched $Pt/Hf:SiO_x/Hf:SiO_x$ (under nitrogen ambient)/TiN devices were fabricated to investigate an accumulation of oxygen ions which induced interface-type switching behavior by introducing nitrogen in the interface between the RRAM active layer and electrode. Types of chemical bonds were analyzed by a Fourier transform infrared spectroscope (FTIR), and current conduction fitting was applied to clarify the physical mechanisms of the effect of oxygen-ion accumulation.

The process sequence was as follows. First, a 300 nm SiO_2 layer was grown by wet oxidation on the lightly doped p-type substrate (100) silicon-substrate. The SiO_2 layer is used as an insulator layer between the bottom electrode and the silicon substrate to block any leakage paths from bottom electrode to silicon substrate. Second, the TiN/Ti bottom electrode of 200 nm was deposited by using RF sputtering and followed by another SiO_2 deposition. The lithography process was performed to pattern the cell size and active region from 0.04 to 64 μm^2. For the introduction of nitrogen between the switching region and active switching region, first a 3 nm $Hf:SiO_x$ thin film was deposited on the patterned $TiN/Ti/SiO_2/Si$ substrate by co-sputtering with pure SiO_2 and Hf targets under argon and nitrogen (50/30 standard cubic centimeter per minute, SCCM) ambient. Then, the 9 nm $Hf:SiO_x$ thin film was deposited under only argon (50 SCCM) ambient. Finally, the 200 nm Pt layer was deposited as top electrode and patterned by a lithography process to form the electrical devices with RRAM sandwich structure, as shown in the bottom left inset of Fig. 1. All of the electrical characteristics were measured by an Agilent B1500 semiconductor analyzer. For all electrical measurements, the bias was applied to the bottom electrode (TiN) as the top electrode (Pt) was grounded.

Fig. 1 shows the electrical current-voltage (I-V) properties and the forming process (bottom right inset of Fig. 1) of typical redox-type resistive switching behavior, which is dominated by an oxygen-ion redox reaction in the RRAM

[a)]Authors to whom correspondence should be addressed. Electronic addresses: tmtsai@faculty.nsysu.edu.tw and tcchang3708@gmail.com.

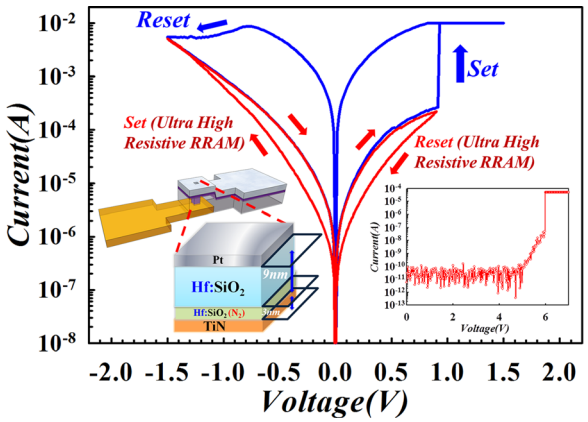

FIG. 1. The I-V characteristic of both traditional redox switching and oxygen-ion accumulation-induced switching behavior. The bottom left inset shows RRAM sandwich structure electrical devices, and bottom right inset shows the I-V characteristic of the forming process.

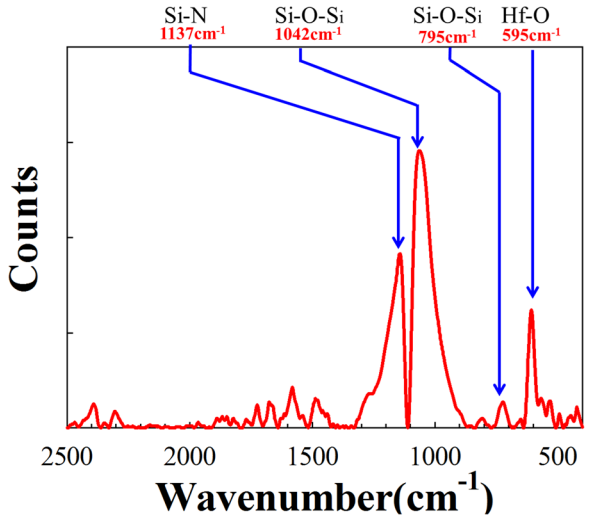

FIG. 2. FTIR spectra of Hf:SiO_x (under nitrogen ambient) film. The Hf-O and Si-N stretch bonding, the anti-symmetric, and symmetric stretch mode of Si-O-Si bonds can be observed.

switching layer (blue line). However, unlike typical resistive switching behaviors, there is a particular phenomenon in our device which exhibits an additional switching behavior at high resistive state (HRS) by applying specific stop voltages. At the HRS of typical resistive switching properties (blue line), there was an additional switching behavior where the "reset" process occurred (red line) when the voltage was swept from 0 V to 0.85 V (which is smaller than the "set" voltage of typical resistive switching properties). In addition, the "set" process occurred when the voltage was swept from 0 V to −1.5 V (red line). This current sub-cycle (red line) was lower than the HRS cycles of typical resistive switching behavior and is defined as an ultra-HRS (UHRS), as shown in Fig. 1.

To analyze the material properties of introducing nitrogen on the interface, FTIR spectroscopy was used. Figure 2 shows the Hf-O stretch bonding found in the Hf:SiO_x (with N_2 ambient) film at 595 cm^{-1}. In addition, the anti-symmetric stretch mode and the symmetric stretch mode of Si-O-Si bonds were discovered at 1042 cm^{-1} and 795 cm^{-1}, respectively. Moreover, the Si-N stretch bonding was also found in the Hf:SiO_x (with N_2 ambient) film at 1137 cm^{-1}. According to these absorption peaks expressed in FTIR spectrums, we can confirm that the Hf element was doped in the silicon oxide film and that by co-sputtering with nitrogen ambient, the N element has been introduced into the Hf:SiO_x film.[43]

To further investigate the reliability of the devices, endurance and retention tests were evaluated in Figs. 3(a) and 3(b). For endurance tests, three resistance states (low resistive state (LRS)/HRS/UHRS) were extracted with a reading voltage of 0.1 V. There was 100 times the resistance ratio between HRS/LRS and 10 times between HRS/UHRS.

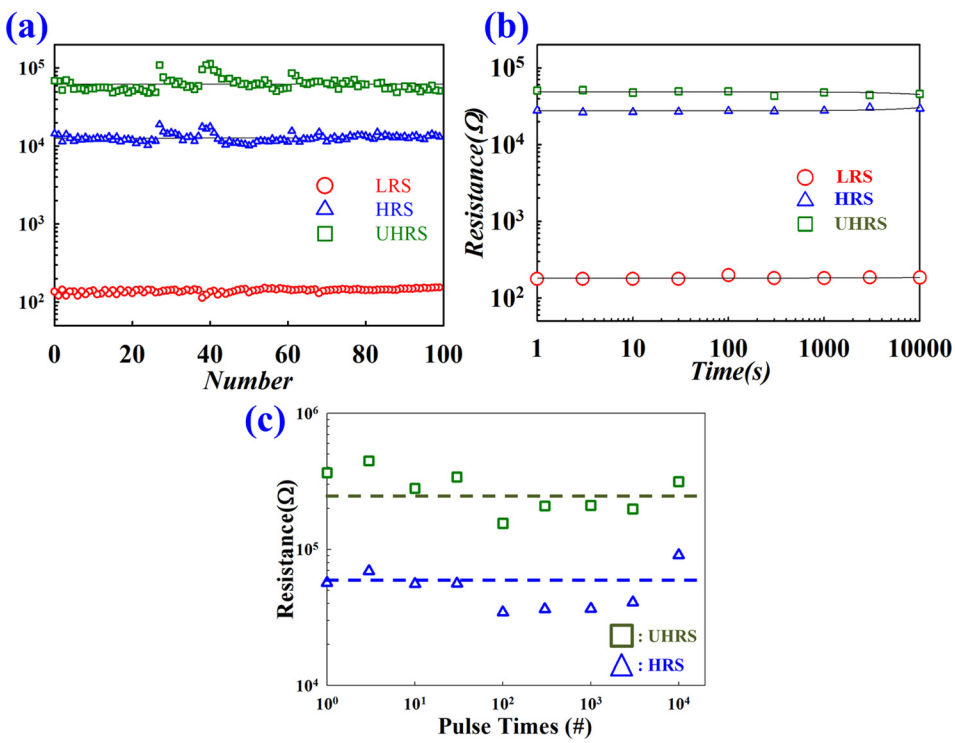

FIG. 3. (a) Three resistance states (LRS/HRS/UHRS) were extracted with a reading voltage of 0.1 V and can be maintained during the 100 cycling bias dc operations. (b) The retention characteristics of LRS, HRS, and UHRS remain almost constant after 10^4 s at 85 °C. (c) The endurance of oxygen-ion accumulation-induced switching characteristics can perform up to 10^4 with UHRS and HRS under AC pulse operation.

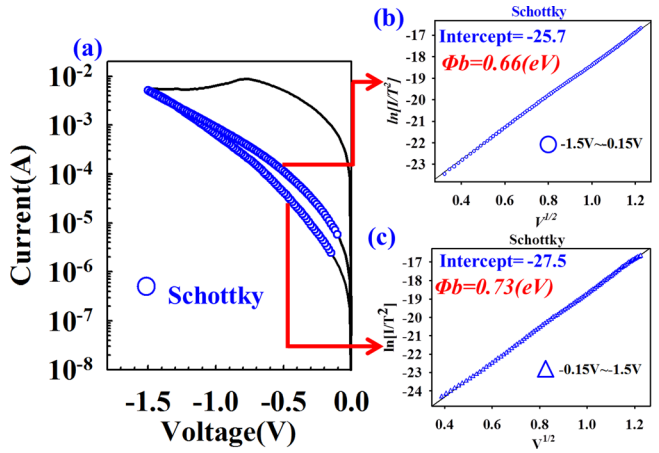

FIG. 4. (a) The current conduction fitting results of HRS and UHRS. (b) A good linear relationship between $V^{1/2}$ and $\ln(I/T^2)$. Based on the intercept, the Schottky barrier height of HRS is 0.66 eV. (c) Based on the intercept, the Schottky barrier height of UHRS is 0.73 eV.

Three resistance states can be maintained during the 100 cycling bias dc operations. The retention performance of the memory device was evaluated at 85 °C by measuring the resistance values of the LRS, HRS, and UHRS at 0.1 V. The resistance values remain almost constant even after 10^4 s. The AC endurance of oxygen-ion accumulation-induced switching characteristics can perform up to 10^4 with UHRS and HRS under AC pulse operation as shown in Fig. 3(c). According to these results, the particular oxygen-ion accumulation-induced switching behavior exhibits stable reliability. Therefore, these devices have potential for RRAM applications because of their low operation power consumption.

The current conduction mechanisms of HRS and UHRS were analyzed in order to further examine the accumulated oxygen-ion switching behavior. The current conduction fitting results are shown in Fig. 4. The relationship in the curve of $\ln(I/T^2)$ versus the square root of the applied voltage ($V^{1/2}$) is linear. This demonstrates that Schottky emission is the main transport mechanism in HRS (−1.5 to −0.15 V) and UHRS (−0.15 to −1.5 V) during the set procedure of the accumulated oxygen-ion switching behavior. The major leakage current arises from the electrons crossing the potential energy barrier between the switching layer and TiN electrode interface by the thermionic effect. According to the Schottky emission formula, $J = A^{**}T^2 \exp\left[\frac{-q(\phi_B - \sqrt{\frac{qV}{4\pi\varepsilon_i d_{sw}}})}{kT}\right]$, where A** is the Richardson constant, with the effective switching thickness (d_{sw}) and energy barrier height (ϕ_B) obtained from the slope and intercept of the plot of $\sqrt{V}$-$\ln\left(\frac{I}{T^2}\right)$, respectively. The slope is $\frac{q}{kT}\sqrt{\frac{q}{4\pi\varepsilon_i d_{sw}}}$ and the intercept is $\ln AA^{**} - \frac{q\phi_B}{kT}$, where $\varepsilon_i = \kappa\varepsilon_0$, and the κ of SiO_2 is about 3.9. The $\ln AA^{**}$ can be ignored because it is much smaller than $\frac{q\phi_B}{kT}$. Using this method, the ϕ_B of HRS and UHRS in Figs. 4(b) and 4(c) can be obtained through calculation, which show that the ϕ_B of HRS and UHRS is about 0.66 eV and 0.73 eV, respectively.

Based on the characteristic of N, which have the lone-pair electrons could capture the oxygen ions.[44] Therefore, the oxygen-ion accumulation induced switching behavior could be easily observed, resulting in good characteristic (UHRS/HRS ratio) and reliability (endurance and retention) on N doped RRAM.

To explain the oxygen-ion accumulation-induced switching behavior in our devices, Figs. 5(a) and 5(b) show band diagrams and schematic diagrams for this particular phenomenon. The device state was after the forming process and being switched to HRS. Fig. 5(a) shows that as an appropriate positive voltage (about 0.9 V, smaller than "set" voltage) is applied, oxygen ions drift to the region then accumulate at the TiN electrode interface. Because of the oxygen-ion (negative charge) accumulation at the interface, the Schottky barrier height increases from 0.66 eV to 0.73 eV. Therefore, the oxygen ion accumulation causes the resistance state to switch from HRS to UHRS. Subsequently, when a negative voltage is applied, oxygen ions are extracted from the accumulation region and redistribute into the silicon oxide film, decreasing the Schottky barrier height (from 0.73 eV to 0.66 eV) and causing the resistance state to switch from UHRS back to HRS, as shown in Fig. 5(b).

In conclusion, both traditional redox switching and oxygen-ion accumulation-induced switching behaviors can be observed in the devices. The latter is induced by introducing nitrogen, which is clarified by material analysis (FTIR), and the reliability of three resistive states (LRS/HRS/UHRS) is also be evaluated by retention and endurance tests. For contrast, traditional redox switching behavior is caused by the

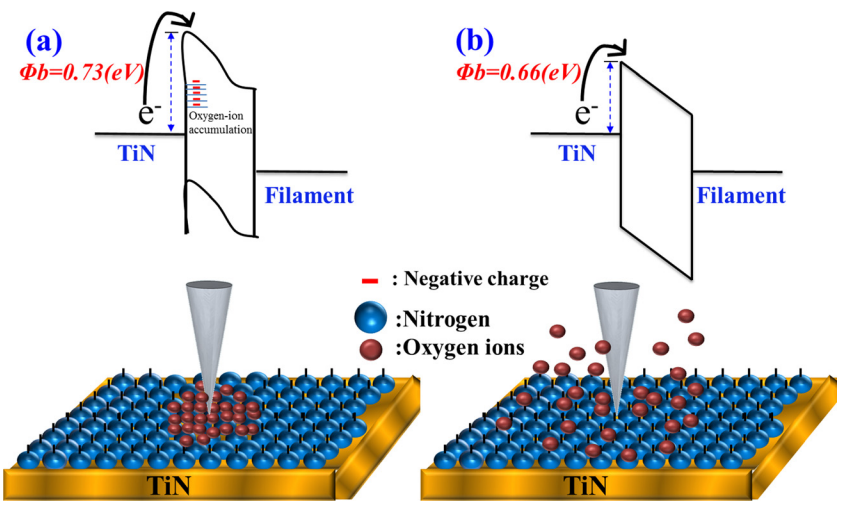

FIG. 5. (a) The band diagram and physics mechanism schematic diagram of the oxygen ions accumulating at the TiN interface. (b) The band diagram and physics mechanism schematic diagram of the extracted and redistributed oxygen ions.

formation and rupture of the conduction path. The oxygen-ion accumulation switching behavior is due to the following mechanism: (1) the dislocated oxygen ions are accumulated in the switching region near the TiN electrode and are extracted from it by applying appropriate positive or negative voltage and (2) as the dislocated oxygen ions (negative charge) are captured by the lone-pair electrons of N and accumulated in the switching region near the TiN electrode, it causes the Schottky barrier height to increase. This oxygen-ion accumulation-induced switching behavior causes the sub-current cycle which is responsible for the UHRS. Therefore, the redox and migration of oxygen ions are the crucial factor for both traditional redox switching and oxygen-ion accumulation switching behaviors being observed in our device. This latter sub-current cycle switching behavior suggests an extraordinary potential in RRAM applications because of its low operation power consumption.

This work was performed at National Science Council Core Facilities Laboratory for Nano-Science and Nano-Technology in Kaohsiung-Pingtung area, NSYSU Center for Nanoscience and Nanotechnology and was supported by the National Science Council of the Republic of China under Contract No. NSC-103-2112-M-110-011-MY3.

[1]M. F. Hung, Y. C. Wu, and Z. Y. Tang, Appl. Phys. Lett. **98**, 162108 (2011).
[2]T. C. Chang, F. Y. Jian, S. C. Chen, and Y. T. Tsai, Mater. Today **14**(12), 608 (2011).
[3]D. D. Jiang, M. H. Zhang, Z. L. Huo, Q. Wang, J. Liu, Z. A. Yu, X. N. Yang, Y. Wang, B. Zhang, J. N. Chen, and M. Liu, Nanotechnology **22**, 254009 (2011).
[4]C. C. Lin and Y. Kuo, J. Appl. Phys. **115**, 084113 (2014).
[5]D. Kahng and S. M. Sze, Bell. Syst. Tech. J. **46**, 1288 (1967).
[6]W. H. Guan, S. B. Long, R. Jia, and M. Liu, Appl. Phys. Lett. **91**, 062111 (2007).
[7]W. Y. Chang, C. S. Peng, C. H. Lin, J. M. Tsai, F. C. Chiu, and Y. L. Chueh, J. Electrochem. Soc. **158**(9), H872 (2011).
[8]Q. Liu, S. B. Long, H. B. Lv, W. Wang, J. B. Niu, Z. L. Huo, J. N. Chen, and M. Liu, ACS Nano **4**(10), 6162 (2010).
[9]T. J. Chu, T. C. Chang, T. M. Tsai, K. C. Chang, Y. E. Syu, G. W. Chang, Y. F. Chang, M. C. Chen, J. H. Lou, J. H. Pan *et al.*, IEEE Electron Device Lett. **34**(4), 502 (2013).
[10]C. H. Hsu, Y. S. Fan, and P. T. Liu, Appl. Phys. Lett. **102**(6), 062905 (2013).
[11]M. Liu, Z. Abid, W. Wang, X. He, Q. Liu, and W. H. Guan, Appl. Phys. Lett. **94**, 233106 (2009).
[12]C. H. Huang, J. S. Huang, S. M. Lin, W. Y. Chang, J. H. He, and Y. L. Chueh, ACS Nano **6**(9), 8407 (2012).
[13]Y. S. Fan, P. T. Liu, L. F. Teng, and C. H. Hsu, Appl. Phys. Lett. **101**, 052901 (2012).
[14]K. C. Chang, T. M. Tsai, T. C. Chang, K. H. Chen, R. Zhang, Z. Y. Wang, J. H. Chen, T. F. Young, M. C. Chen, T. J. Chu *et al.*, IEEE Electron Device Lett. **35**(5), 530 (2014).
[15]S. B. Long, X. J. Lian, C. Cagli, L. Perniola, E. Miranda, M. Liu, and J. Sune, IEEE Electron Device Lett. **34**(8), 999 (2013).
[16]R. Zhang, K. C. Chang, T. C. Chang, T. M. Tsai, S. Y. Huang, W. J. Chen, K. H. Chen, J. C. Lou, J. H. Chen, T. F. Young *et al.*, IEEE Electron Device Lett. **35**(6), 630 (2014).
[17]H. T. Sun, H. B. Lv, Q. Liu, S. B. Long, M. Wang, H. W. Xie, X. Y. Liu, X. Y. Yang, J. B. Niu, and M. Liu, IEEE Electron Device Lett. **34**(7), 873 (2013).
[18]S. B. Long, X. J. Lian, T. C. Ye, C. Cagli, L. Perniola, E. Miranda, M. Liu, and J. Sune, IEEE Electron Device Lett. **34**(5), 623 (2013).
[19]C. C. Shih, K. C. Chang, T. C. Chang, T. M. Tsai, R. Zhang, J. H. Chen, K. H. Chen, T. F. Young, H. L. Chen, J. C. Lou *et al.*, IEEE Electron Device Lett. **35**(6), 633 (2014).
[20]K. C. Chang, T. M. Tsai, T. C. Chang, H. H. Wu, K. H. Chen, J. H. Chen, T. F. Young, T. J. Chu, J. Y. Chen, C. H. Pan *et al.*, IEEE Electron Device Lett. **34**(4), 511 (2013).
[21]S. B. Long, L. Perniola, C. Cagli, J. Buckley, X. J. Lian, E. Miranda, F. Pan, M. Liu, and J. Sune, Sci. Rep. **3**, 2929 (2013).
[22]K. C. Chang, T. M. Tsai, R. Zhang, T. C. Chang, K. H. Chen, J. H. Chen, T. F. Young, J. C. Lou, T. J. Chu, C. C. Shih *et al.*, Appl. Phys. Lett. **103**, 083509 (2013).
[23]H. B. Lv, Y. T. Li, Q. Liu, S. B. Long, L. Li, and M. Liu, IEEE Electron Device Lett. **34**(2), 229 (2013).
[24]W. H. Guan, S. B. Long, Q. Liu, M. Liu, and W. Wang, IEEE Electron Devices Lett. **29**(5), 434 (2008).
[25]K. C. Chang, R. Zhang, T. C. Chang, T. M. Tsai, J. C. Lou, J. H. Chen, T. F. Young, M. C. Chen, Y. L. Yang, Y. C. Pan *et al.*, IEEE Electron Device Lett. **34**(5), 677 (2013).
[26]S. B. Long, X. J. Lian, C. Cagli, X. Cartoixa, R. Rurali, E. Miranda, D. Jimenez, L. Perniola, M. Liu, and J. Sune, Appl. Phys. Lett. **102**(18), 183505 (2013).
[27]K. C. Chang, C. H. Pan, T. C. Chang, T. M. Tsai, R. Zhang, J. C. Lou, T. F. Young, J. H. Chen, C. C. Shih, T. J. Chu *et al.*, IEEE Electron Device Lett. **34**(5), 617 (2013).
[28]Q. Liu, S. B. Long, W. Wang, Q. Y. Zuo, S. Zhang, J. N. Chen, and M. Liu, IEEE Electron Device Lett. **30**(12), 1335 (2009).
[29]T. M. Tsai, K. C. Chang, T. C. Chang, Y. E. Syu, K. H. Liao, B. H. Tseng, and S. M. Sze, Appl. Phys. Lett. **101**, 112906 (2012).
[30]Y. E. Syu, T. C. Chang, J. H. Lou, T. M. Tsai, K. C. Chang, M. J. Tsai, Y. L. Wang, M. Liu, and Simon M. Sze, Appl. Phys. Lett. **102**, 172903 (2013).
[31]Y. Wang, Q. Liu, S. B. Long, W. Wang, Q. Wang, M. H. Zhang, S. Zhang, Y. T. Li, Q. Y. Zuo, and J. H. Yang, Nanotechnology **21**, 045202 (2010).
[32]Y. J. Chen, K. C. Chang, T. C. Chang, H. L. Chen, T. F. Young, T. M. Tsai, R. Zhang, T. J. Chu, J. F. Ciou, J. C. Lou *et al.*, IEEE Electron Device Lett. **35**(10), 1016 (2014).
[33]Y. T. Li, S. B. Long, M. H. Zhang, Q. Liu, S. Zhang, Y. Wang, Q. Y. Zuo, S. Liu, and M. Liu, IEEE Electron Device Lett. **31**(2), 117 (2010).
[34]Y. T. Su, K. C. Chang, T. C. Chang, T. M. Tsai, R. Zhang, J. C. Lou, J. H. Chen, T. F. Young, K. H. Chen, B. H. Tseng *et al.*, Appl. Phys. Lett. **103**, 163502 (2013).
[35]W. T. Lian, H. B. Lv, Q. Liu, S. B. Long, W. Wang, Y. Wang, Y. T. Li, S. Zhang, Y. H. Dai, J. N. Chen *et al.*, IEEE Electron Device Lett. **32**(8), 1053 (2011).
[36]K. C. Chang, T. M. Tsai, T. C. Chang, H. H. Wu, J. H. Chen, Y. E. Syu, G. W. Chang, T. J. Chu, G. R. Liu, and Y. T. Su, IEEE Electron Device Lett. **34**(3), 399 (2013).
[37]T. M. Tsai, K. C. Chang, R. Zhang, T. C. Chang, J. C. Lou, J. H. Chen, T. F. Young, B. H. Tseng, C. C. Shih, Y. C. Pan *et al.*, Appl. Phys. Lett. **102**, 253509 (2013).
[38]R. Zhang, K. C. Chang, T. C. Chang, T. M. Tsai, K. H. Chen, J. C. Lou, J. H. Chen, T. F. Young, C. C. Shih, and Y. L. Yang, Nanoscale Res. Lett. **8**, 497 (2013).
[39]T. M. Tsai, K. C. Chang, T. C. Chang, Y. E. Syu, S. L. Chuang, G. W. Chang, G. R. Liu, M. C. Chen, H. C. Huang, S. K. Liu *et al.*, IEEE Electron Device Lett. **33**(12), 1696 (2012).
[40]T. M. Tsai, K. C. Chang, T. C. Chang, G. W. Chang, Y. E. Syu, Y. T. Su, G. R. Liu, K. H. Liao, M. C. Chen, H. C. Huang *et al.*, IEEE Electron Device Lett. **33**(12), 1693 (2012).
[41]Y. E. Syu, T. C. Chang, T. M. Tsai, Y. C. Hung, K. C. Chang, M. J. Tsai, M. J. Kao, and S. M. Sze, IEEE Electron Device Lett. **32**(4), 545 (2011).
[42]T. J. Chu, T. M. Tsai, T. C. Chang, K. C. Chang, R. Zhang, K. H. Chen, J. H. Chen, T. F. Young, J. W. Huang, J. C. Lou *et al.*, IEEE Electron Device Lett. **35**(2), 217 (2014).
[43]S. Kanga, S. Honga, C. R. Choeb, M. Parkb, S. Rimb, and J. Kimb, Polymer **42**(3), 879 (2001).
[44]Y. E. Syu, R. Zhang, T. C. Chang, T. M. Tsai, K. C. Chang, J. C. Lou, T. F. Young, J. H. Chen, M. C. Chen, Y. L. Yang *et al.*, IEEE Electron Device Lett. **34**(7), 864 (2013).